HHS Public Access

Author manuscript

Phys Med Biol. Author manuscript; available in PMC 2017 March 07.

Published in final edited form as:

Phys Med Biol. 2016 March 7; 61(5): R32–R56. doi:10.1088/0031-9155/61/5/R32.

Motion correction in MRI of the brain

F Godenschweger[1], **U Kägebein**[1], **D Stucht**[1,2], **U Yarach**[1,3], **A Sciarra**[1], **R Yakupov**[1], **F Lüsebrink**[1], **P Schulze**[1,6], and **O Speck**[1,4,5,6]

F Godenschweger: frank.godenschweger@ovgu.de

[1]Biomedical Magnetic Resonance, Otto-von-Guericke University, Magdeburg, Germany [2]Institute of Biometry and Medical Informatics, Otto-von-Guericke University, Magdeburg, Germany [3]Department of Radiological Technology, Chiangmai University, Chiang Mai, Thailand [4]Center for Behavioral Brain Sciences, Magdeburg, Germany [5]Leibniz Institute for Neurobiology, Magdeburg, Germany [6]German Center for Neurodegenerative Disease (DZNE), site Magdeburg, Germany

Abstract

Subject motion in MRI is a relevant problem in the daily clinical routine as well as in scientific studies. Since the beginning of clinical use of MRI, many research groups have developed methods to suppress or correct motion artefacts. This review focuses on rigid body motion correction of head and brain MRI and its application in diagnosis and research. It explains the sources and types of motion and related artefacts, classifies and describes existing techniques for motion detection, compensation and correction and lists established and experimental approaches. Retrospective motion correction modifies the MR image data during the reconstruction, while prospective motion correction performs an adaptive update of the data acquisition. Differences, benefits and drawbacks of different motion correction methods are discussed.

Keywords

motion artefact; motion tracking; optical tracking; navigator; cross calibration; prospective/retrospective motion correction; MRI

1. Introduction

Magnetic resonance imaging (MRI) is an indispensable tool for medical diagnosis offering detailed visualization of the inner structure of the human body, the extremities as well as the brain. In particular, high field MRI became an important modality for research in neuroscience due to its non-invasiveness. The wide variety of MR imaging methods enables high spatial resolution imaging and allows encoding of various contrast mechanisms. This enables to distinguish many types of human soft tissue such as brain, abdominal organs, muscle fibres, ligament and sinew, blood vessels etc. and renders MRI superior to many other imaging modalities in the detection and characterization of soft tissue pathologies. Despite these obvious advantages of MRI, many difficulties in clinical and research

Some figures may appear in colour only in the online journal

applications of MRI arise from relatively long data acquisition times. Other issues, such as the high complexity of MRI and required expertise, contraindications due to implants, costs and others are not considered in this review that focuses on the motion-related challenges and solutions.

Imaging with MR is time consuming due to the sequential acquisition of the 1D MR-signal. Consequently MRI is sensitive to motion. Patient or subject motion during the acquisition can induce artefacts and reduce image quality and diagnostic or scientific relevance. Such motion artefacts manifest as ghosting, blurring, geometric distortion or decreased signal-to-noise ratio (SNR). For diagnosis, their clinical relevance depends on the reader's ability to identify and separate such artefacts from the structure of interest and the obstruction or mimicking of pathologies. Automated quantitative data analysis may be corrupted even more severely. Image quality degradation may result in non-diagnostic data and require repetition of a single scan or the entire session leading to a delay of treatment and rising costs. If unnoticed, potential false positive or negative findings may occur (Andre *et al* 2015).

For more than 30 years and since the beginning of clinical use of MRI, many research groups have developed methods to prevent, suppress or correct motion artefacts. An obvious method is the reduction of image acquisition time. Fast imaging methods have been and are still the focus of research and imaging times have come down from dozens of minutes for single volume acquisitions to only a few minutes or seconds. Further reduction of imaging time, however, often leads to compromises in resolution, contrast or signal-to-noise ratio.

Active methods for the correction of motion are required and may be categorized according to different criteria (see figure 1). The type of motion can be rigid (translation, rotation) or deformable (non-rigid). The motion can occur between volumes (inter-image), within a volume between excitation pulses (inter-scan) or between excitation and signal acquisition (intra-scan). Commonly, the amount of motion during a certain acquisition time period (e.g. total scan time, single slice, single k-space line) in relation to the spatial resolution is relevant. The motion pattern can be periodic, quasi-periodic, continuous or sporadic/random. In 2D-imaging, motion within the excited slice plane is termed in-plane motion, whereas motion perpendicular to the slice is termed through-plane motion (Boussel *et al* 2006). In non-selective 3D imaging the differentiation between in-plane and through-plane motion is not required.

The prevention or correction of motion-induced artefacts in brain MRI is an important objective. Other fields of motion artefact correction are cardiac, liver and thorax MRI, however, with only limited overlap in methodological approaches with head motion correction due to the nature of the periodic motion of the heart and chest. This review aims at an overview of state-of-the-art techniques for the correction of motion induced artefacts. The main focus is the motion correction of MRI of the brain, where many methods have been developed. In section 2 the sources and types of motion and related MRI artefacts are described. Section 3 presents a description of techniques to detect and classify motion. The following two sections 4 and 5, discuss retrospective and prospective motion correction approaches. The correction of residual artefacts after the correction of rigid body motion is shown in section 6.

2. Relevant motion and related artefacts in MRI

Sources of motion in human subjects are of physiological nature. We can categorize such physiological sources as (i) periodic involuntary motion, such as cardiac, respiratory, and peristaltic motion including related flow of blood and cerebrospinal fluid (CSF), (ii) sudden involuntary movements caused by sneezing, coughing, yawning, and semi-regular movements such as swallowing and blinking, or (iii) conscious motion of body parts, e.g. due to discomfort or carelessness of the subjects. Patients affected by neurodegenerative diseases, such as Parkinson's, can present with tremor. Non-compliant subjects, e.g. children, tend to move more.

While motion artefacts are the most prevalent cause for MRI image quality degradation, other artefacts may also corrupt MRI acquisitions. A classification of the artefact sources in MRI may refer to these 3 categories (Heiland 2008):

- **i.** Hardware-related artefacts: e.g. spikes, data clipping, zippers, and other artefacts due to external RF sources;
- **ii.** Sequence-related artefacts: aliasing, partial volume effects, crosstalk between slices, saturation artefacts, chemical shift artefacts, truncation artefacts (Gibbs ringing), echo planar imaging (EPI) ghosting;
- **iii.** Patient-related artefacts: *motion artefacts*, susceptibility artefacts;

For a better understanding of the effects of motion on MR images, it is helpful to consider the image formation process (for physical artefact description see also (Zaitsev *et al* 2015)).

The signals acquired in MRI are spatially encoded by the application of imaging gradients. These raw data are stored in the so-called *k*-space domain and the corresponding *k*-space coordinate of each measurement point is given by the gradient moment (Paschal and Morris 2004):

$$k_x(t)=\gamma\int_0^t G_x(x,t')\mathrm{d}t'. \quad (1)$$

Applying an inverse Fourier transformation to the acquired *k*-space data $S(k_x, k_y, k_z)$ results in the final image $I(x,y,z)$

$$I(x,y,z)=\iiint S(k_x,k_y,k_z).\mathrm{e}^{\mathrm{i}2\pi(xk_x+yk_y+zk_z)}\mathrm{d}k_x\mathrm{d}k_y\mathrm{d}k_z. \quad (2)$$

By nature of the Fourier transform, each pixel in the MR image is the weighted sum of all points in *k*-space. The coordinates of the raw data points in *k*-space and the order of their sequential acquisition are termed sampling scheme or trajectory. Most commonly, Cartesian coordinates are sampled but other trajectories, such as spiral or radial may be applied (Hennig 1999) (see also section 3.1). Changes of the raw data phase or amplitude as well as the *k*-space position due to motion can affect the entire image, depending on the motion pattern, the contrast encoding, and the sampling scheme. The relation between pose changes

in the spatial domain and resulting changes of *k*-space data acquired during this pose is important in this context. According to the Fourier shift theorem, object translation causes a linear phase ramp in the *k*-space data in the direction of motion. Object rotation, however, results in identical rotation of the *k*-space data (Hennig 1999, Bernstein *et al* 2004, Paschal and Morris 2004, Heiland 2008). In addition, motion can cause further signal changes such as signal amplitude variation due to spin history effects (saturation), signal phase variation due to position dependent Larmor frequency differences, and phase accumulation when the displacement occurs during and in the direction of a magnetic field gradient.

As a consequence of inter-scan motion *k*-space data from different positions are combined and signal intensities may change due to spin history effects leading to inconsistent *k*-space data. In addition, intra-scan motion can further affect the signal phase. Position is encoded in the signal phase and thus, false positions and again inconsistent data arise. For Cartesian sampling schemes with fast acquisition in the read encoding direction, these inconsistencies appear mainly along the phase encoding direction. As a result motion related artefacts spread along this phase encoding direction, independent of the direction of motion (see figure 2).

Depending on the motion pattern and sequence, ghosting, blurring or local signal variation occurs in the reconstructed image. Ghosting effects, where object structures are repeatedly appearing in the image, are usually caused by (quasi-) periodic motion. This can also be understood as a result of Fourier transform properties. The Fourier transform of a periodic signal modulation contains extra peaks besides the DC peak, which represents the signal integral. According to the Fourier convolution theorem, a signal modulation (multiplication) is equivalent to a convolution of the Fourier transforms of the original object and the signal modulation. A (quasi-) periodically moving structure will therefore be represented multiple times in the reconstructed image (see figure 3(a)). Less structured signal modulation in *k*-space, i.e. random motion patterns typically leads to blurring of sharp edges in the image (see figure 3(b)) and motion induced phase changes can result in destructive interference and signal loss. If unsaturated magnetization enters the measurement volume due to through-plane motion, the signal intensity will change similarly to the inflow effect in time-of-flight angiography (see figure 3(d)).

Another approach to understand motion induced imaging effects has been proposed by Shechter and McVeigh (2003) who presented a 3D affine motion model for deformable object motion. This model considers 12 degrees of freedom, including translation and rotation as well as shearing and scaling. Lauzon and Rutt (1993) proposed a *k*–*t*-space formalism based on the Fourier projection slice theorem in order to predict how motion artefacts arise. Batchelor *et al* (2005) introduced a matrix description for general motion correction in multi-shot imaging.

3. Motion detection techniques

Independent of the correction techniques the object or subject movement needs to be known or estimated in order to correct for it. In the following sections we will focus on the detection and correction of rigid body motion. With that assumption only a small number of

parameters are required to fully describe the object pose. In general these are six parameters to describe position and orientation of an object from which the translational and rotational motion between time points can be determined. If motion is restricted or assumed to be only 1D, this reduces to one position parameter and if motion is assumed to be 2D, two position and one orientation parameters are needed.

The methods for rigid body pose or motion detection are classified in MR-based, RF-based, and optical motion tracking categories and described in more detail in the following sections.

3.1. MR-based motion tracking

The MR-based methods are historically the first to track motion. These methods acquire at least two MR data sets at different time points and compare these data to determine motion without the need for additional hardware. The pose changes can be calculated by registration algorithms or by comparison to training data sets on the basis of 3D volumes, slices or 1D, 2D or 3D navigators.

3.1.1. Navigators—In the following sections we describe three navigator principles: self-navigation, navigator echoes, and coil sensitivities.

3.1.1.1. Self-navigation: Self-navigation techniques estimate the motion directly from the acquired imaging data using *k*-space trajectories that sample parts of *k*-space repeatedly (see figure 4). The most popular self-navigation technique is PROPELLER (Pipe 1999), which can measure in-plane translation as well as rotation and can reject data indicating through-plane motion. Concentrically rotating rectangular blocks of *k*-space are sampled, consisting of distinct parallel linear trajectories. Thus, a central circle around the *k*-space origin is re-sampled with each block or blade and the data from the overlapping region are used for motion determination. This redundant central data portion represents a low resolution image of the slice, which is updated with every block and saved for registration. The motion information between blocks is used to correct each block during reconstruction. The main drawbacks of PROPELLER are reduced efficiency compared to Cartesian sampling due to the need for more sampling points and its sensitivity to gradient timing delays and field inhomogeneities that can lead to inconsistencies in the blocks with changing orientation even without object motion. Furthermore, the method assumes minimal motion during the acquisition of each block and only corrects for motion between blocks. PROPELLER has been one of the few methods that have been adopted by all major vendors into their products as motion-robust acquisition methods.

Another self-navigation technique proposed by Bookwalter *et al* (2010) is the multiple overlapping *k*-space junctions for investigating translating objects (MOJITO). Through the use of intersecting *k*-space trajectories (BOWTIE trajectory) and the phase differences occurring at the intersection points, in-plane translation can be detected. It requires uniform coil sensitivity and motion-free acquisition of reference lines.

Instead of using self-navigating 2D *k*-space sub-trajectories, Gai *et al* (1996), Shankaranarayanan *et al* (2001) and Vaillant *et al* (2014) applied radial 1D trajectories (also

called projection reconstruction) which result in more variability regarding temporal resolution and overlap region. They determined in-plane translation using a certain consistency condition (e.g. Ludwig–Helgason condition). The algorithm of Welch *et al* (2004) is also using a radial MR trajectory. For the additional determination of the in-plane rotational motion of an imaged object they used the 2nd moments of the spatial domain projections. In the proposed view angle acquisition order, the acquisition is self-navigating with respect to both in-plane translation and rotation. Anderson *et al* (2011) further advanced the radial trajectory technique for translational and rotational motion detection by ordering the views correspondingly. They are using subsets of motion affected and motion free data to estimate the motion with the registration scheme from (Jenkinson and Smith 2001).

Liu *et al* (2004) explored the self-navigated interleaved spiral (SNAILS) trajectories for diffusion tensor imaging. The *k*-space is recorded with interleaved variable-density (VD) spiral readout trajectories oversampling the centre of *k*-space to determine the motion between spirals. After each VD spiral interleave, a phase error is estimated from the low-resolution images allowing estimation of in-plane translational motion similar to PROPELLER.

3.1.1.2. Navigator echoes: Instead of changing the sampling scheme, motion information can be determined using additional data collection (navigator echoes), typically at the beginning or at the end of the repetition loop. The extra data acquisition requires additional time, prolonging the minimal repetition time (TR) and leading to reduction in efficiency (Fu *et al* 1995, Robson *et al* 1997, McGee *et al* 2000b, Bookwalter *et al* 2010).

The first navigator echo sequence, measuring translational in-plane motion, was proposed by Ehman and Felmlee (1989). The navigator (NAV) echo is a phase-encoding free image projection along the *x*-axis or/and *y*-axis inserted between two consecutive refocusing RF pulses (see figure 5). If motion exists, the linear NAV echo will vary. However, it assumes a single moving object within the FoV and it cannot measure rotation as well as translation in *z*-direction (Fu *et al* 1995). Hu *et al* (1994) used a single data point in a gradient echo sequence instead of a full NAV echo to detect signal fluctuations in functional imaging. The linear NAV echo technique was further extended to measure small head motions in DTI assuming translation and rotation along the readout direction. This technique is called single shot navigation (Anderson and Gore 1994, Ordidge *et al* 1994, de Crespigny *et al* 1995). However, motion along the phase-encoding direction is not detectable by single shot navigation. Therefore, Butts *et al* (1996) introduced the time-efficient orthogonal NAV echoes for multi-shot diffusion-weighted echo planar sequences.

The navigator echo technique was further expanded to orbital navigators being centred at the origin of *k*-space by Fu *et al* (1995) and improved by Ward *et al* (2000). They estimated inter-scan in-plane 2D translational and rotational motion from the raw data of an orbital navigator echo. Rotations shift the magnitude profile along the echo, which is circular in *k*-space, whereas translations cause phase differences between the first and current navigator echo. Similar approaches with different trajectories in *k*-space are octant navigators proposed by van der Kouwe *et al* (2001) and spherical navigators by Welch *et al* (2002).

A further improvement of the previously mentioned navigators is the cloverleaf navigator from van der Kouwe *et al* (2006). They minimized the through-plane motion artefacts of the previous approaches using a preparation map of 378 navigators in different directions from which they estimate the nearest representative.

Another approach by Lin *et al* (2010) is called floating navigator echoes. They introduced a combination of navigator echoes with generalized auto-calibrating partially parallel acquisition (GRAPPA) to measure in-plane and through-plane translational and rotational motion.

3.1.1.3. Coil sensitivities: The use of multiple receiver coils in MR has led to an improvement in image signal-to-noise and allowed the reduction of measurement time through parallel imaging methods. Bydder *et al* (2002) first proposed a technique using Cartesian sensitivity encoding (SENSE) to measure in-plane translational motion between subsets of the data. The acquired *k*-space data are split into odd and even lines. Using SENSE, full *k*-space data sets are reconstructed, which results in multiple copies of *k*-space. The data sets are iteratively compared to each other to detect motion induced inconsistencies. The obvious penalty is noise amplification in the parallel imaging reconstruction process.

Aksoy *et al* (2006) and Bammer *et al* (2007) presented a combination of spiral navigator images with SENSE reconstruction for in-plane translation and rotation detection. All navigator images are co-registered to a reference navigator image to obtain the amount of translation and rotation through optimizing a corresponding cost function.

Kober *et al* (2011) used free induction decay signals without any additional gradient encoding (FID Navigator) to detect motion of the brain. By using a high number of receiver coils and applying ultra-short (<100 μs) FID signals, the variation of the FID signals of every coil provides a sensitive measure of motion which can be used to reject motion corrupted data (Loktyushin *et al* 2013). Including the FID navigator into the sequence results in a minor time penalty of less than 1 ms.

3.1.2. Image-based motion tracking—If multiple consecutive volumes are acquired in a single study they can be corrected against each other. This is the case, e.g. in functional MRI, perfusion MRI, diffusion weighted MRI or when multiple averages are needed. The motion between such volumes can be determined through registration methods. In functional MRI usually a full 3D estimation of head movement is calculated for every volume with respect to a reference volume, e.g. the first time point or a time-averaged volume. The basic principle of registration is the process of finding a rigid body transformation between two images or volumes through an optimization algorithm by minimizing a global image similarity metric (e.g. mutual information, signal differences, etc). This purely image-based motion detection assumes that significant motion occurs only between volume acquisitions (Kim *et al* 2010). Complete volumes instead of single *k*-space lines can be retrospectively corrected by image interpolation. If the motion information is calculated quickly enough each following volume acquisition can be adapted to let the acquisition volume follow the motion as proposed by Thesen *et al* (2000).

Refined approaches for image-based motion tracking use multi-slice axial MRI data sets (figure 6) (Jiang *et al* 1995, Mangin *et al* 2002, Kochunov *et al* 2006, Bertelsen *et al* 2009). A stack of images (*stack-to-volume*) or individual slices (*slice-to-volume*) are selected from the data set. Using image registration software, e.g. FLIRT (Jenkinson *et al* 2002) or SPM (Kochunov *et al* 2006) a 6D transformation relative to a reference volume (e.g. previously acquired high-resolution volume (Kim *et al* 1999)) is determined via a registration algorithm. The disadvantage of these techniques is the quality dependency on the reference image. This could be improved by a group-wise approach taking the intensity distributions of all images simultaneously into account (Huizinga *et al* 2014). A group-wise registration can be performed using various algorithms such as voxel-wise variance (Metz *et al* 2011), minimum description length (Marsland *et al* 2008), multivariate similarity measure (Wachinger and Navab 2013), stack entropy cost function (Miller *et al* 2000) or dissimilarity measure (Huizinga *et al* 2014). Due to the fact that only multiple stacks in a single orientation are considered, through-plane motion cannot be detected (Kim *et al* 2010).

An approach for the acquisition of motion corrected high resolution MRI volumes of fetal brains was proposed by Rousseau *et al* (2005). Motion is estimated by iterative registration of multiple orthogonal sets of fast 2D MRI slices, which are fairly robust to motion. A refined approach for 3D reconstruction using the slice intersection method was proposed by Kim *et al* (2010) (see also the review for mapping fast fetal brain imaging by Studholme (2011)).

The slice intersection method considers multiple motion corrupted 2D MR images in three approximately orthogonal directions. The motion is detected within a conventional optimization problem using the intersecting intensity profiles of orthogonally located slice pairs. Failures during the registration process can arise from inhomogeneous bias fields, noise or partial volume effects (Cheng *et al* 2012). Full image navigators have been proposed by White *et al* (2010) who applied three orthogonal fast spiral navigator images to estimate motion between navigators through image registration of following images. Tisdall *et al* (2012) used EPI as a volume navigator in order to obtain the head motion information during MP-RAGE acquisitions. Since these navigator acquisitions are time consuming and affect the magnetization state, they can only be inserted in sequences that contain sufficient unused time, such as 3D TSE or MP-RAGE.

3.2. RF-based tracking systems

RF-based tracking or field detection methods have a long history in MRI. While the methods described above all rely on the standard MRI system without the need for additional hardware, these methods employ additional small pickup coils with very local sensitivity that are recorded in additional RF receivers. The position of such small coils can be encoded in the signal frequency when received in the presence of a gradient. For 3D position encoding, three separate gradients need to be applied. Therefore, similar to navigator methods, additional time is needed in the sequence. As only the position and not the orientation of a single coil can be encoded, three such coils need to be attached to the object to determine its rigid body pose and motion.

The RF-based technique was first introduced 1986 for tracking of devices in interventional MRI by Ackerman *et al* (1986). A real-time approach was developed by Dumoulin *et al* (1993). *The first application to motion tracking in MRI was published by* Derbyshire *et al* (1998).

More recently, Krueger *et al* (2006) and Ooi *et al* (2009) used two or more tracking coils termed active markers. They estimated object movement from comparison of periodic updates of the marker positions (Umeyama 1991). The additional RF excitation, encoding gradients, and spoiler for background suppression required approximately 15 ms for each update. These were the first approaches to real-time correction of intra-scan motion.

Improvements of the active markers were presented by Ooi *et al* (2011, 2013b) and Sengupta *et al* (2013) including wireless instead of wired pickup coils resulting in more convenient handling and improved safety but added challenge to assign marker signals to each coil.

van der Kouwe *et al* (2009) proposed the EndoScout gradient-based tracking system with small pickup coils placed on each face of a small cubic sensor for motion detection. This sensor does not directly employ the resonance signal but the change in magnetic field that induces a voltage in the coils during gradient switching from which the position and orientation of the sensor inside the scanner bore is determined.

A variant has been proposed by Qin *et al* (2013) and was applied to calculate 3D motion with intracavity imaging coils. Here four tracking coils were distributed in a tetrahedral configuration to provide isotropic resolution of translation and rotation.

3.3. Optical tracking systems

Optical tracking systems use cameras for motion tracking of known markers inside the MRI system. A well-known optical motion tracking system is based on multiple cameras and stereoscopic reconstruction. A number of such systems are used in the motion picture industry or in surgery to track devices or patient position. In 2005 Tremblay *et al* (2005) applied an infrared tracking system within the MR environment. Two cameras placed at known positions outside the scanner bore detected three or four reflective markers. Using parallax calculations position and orientation in 6 degrees of freedom was determined entirely independent of the MRI system.

A similar approach was published by Zaitsev *et al* (2006). They use a stereoscopic infrared tracking system positioned outside the MR scanner and reflective markers. The main limitations of these methods are the large distance of the cameras from the tracking target and the small angle between the views of less than 20°. These reduce the possible accuracy of the tracking data. In addition, at least three markers are required to obtain 3D motion information.

To improve tracking accuracy Qin *et al* (2009) mounted two cameras inside the scanner bore to the head coil and thus much closer to the marker and with larger view angle. Because of the limited space the cameras and lenses were miniaturized but still a rigid target with multiple markers was required. Schulz *et al* (2012) extended this approach using three cameras mounted at close distance to the head, each viewing only one marker.

More recently, single camera systems have gained more interest due to their smaller footprint and simpler handling. With only one camera the requirements for a line of sight are reduced and calibration is simplified since the geometry between multiple cameras does need extra consideration. With a single camera, however, additional information needs to be encoded through the marker. A checkerboard, for example, contains many feature points with known geometry and was proposed by Aksoy (2010) together with a single camera mounted to the head coil. The large self-encoded marker is visible to the camera for a large range of motion even at close distance. To resolve ambiguities in the regular pattern, each square of the checkerboard contains a binary code to encode position information of each square on the marker (see Forman *et al* (2011)). The authors quote a tracking precision of ~0.1 mm in translation and ~0.1° in rotation.

Maclaren *et al* (2012) introduced another single camera tracking system mounted inside the scanner bore tracking a single small 15 mm marker. The moiré phase tracking (MPT) is based on moiré patterns generated by gratings on both sides of a transparent substrate. The phase of these patterns is generated by interference between the gratings and very sensitive to rotations. The accuracy reported by the authors is ~0.01 mm in translation and ~0.01° in rotation.

3.3.1. Cross calibration—All methods described at the beginning of this chapter (navigators, RF-tracking) use gradients to encode position and thus intrinsically report positions in MR scanner coordinates. In contrast, optical tracking systems obtain pose information in their own coordinate system. These coordinates need to be transformed to the MR scanner's coordinate system. The process to determine the corresponding transformation matrix is referred to as cross calibration. It is an important and critical process regarding the accuracy of motion tracking.

Several methods for the determination of this transformation matrix have been presented. In robotics, this is termed the hand-eye coordination problem. One approach is to acquire 3D data of a phantom with internal structure by MRI with simultaneous pose tracking of a marker attached to this phantom by the external tracking system. If the spatial relation between the phantom and the marker is known, a cross calibration matrix can be calculated (Aksoy *et al* 2012). If the relation is unknown, an iterative approach can be used, where the object is imaged at multiple positions with MRI and the tracking system. Image based co-registration delivers pose changes. The difference between the image based pose changes and the pose data of the external tracking system is then minimized iteratively (Zaitsev *et al* 2006) or in a non-iterative process (Kadashevich *et al* 2011) leading to an estimate of the coordinate transformation matrix. Instead of using image based registration, the position and orientation changes of a phantom can also be calculated directly from two MR images at different phantom poses provided that the phantom contains sufficiently unique features (Zahneisen *et al* 2014).

Important criteria for any tracking technique are precision, accuracy, and latency as analyzed by Maclaren *et al* (2013). The authors define precision as the level of jitter or noise (reproducibility of the measurement), accuracy as the discrepancy of the measured and the true pose and latency as the delay between motion occurrence and availability of the

tracking data or MR pose update. The methods described above have advantages and shortcomings regarding these tracking quality criteria that depend not only on the measurement principle but also largely on the specific implementation. For any practical application, the convenience of operation also needs to be considered. MR navigator-based methods generally do not require the attachment of markers (optical or RF-coils) to the subject and are thus more convenient. If markers are required, the quality of the tracking data is often limited by the rigidity of the marker attachment. With optical tracking the range of trackable motion can be limited by line-of-sight requirements. A redundant multi-camera or multi-marker approach can increase the possible range of motion (Singh *et al* 2015).

4. Retrospective motion correction

Retrospective motion correction refers to a group of correction methods that modify the MR *k*-space or image data after acquisition, i.e. during reconstruction. The acquisition itself is performed independent of potential motion. Object motion is either known through additional detection techniques as described above or estimated from the data itself.

4.1. Prior information-based motion correction

If motion is known through any of the tracking methods described above, some of the effects of motion can be ‘undone’ during reconstruction. These mainly include correction of the effects of translation and rotation on *k*-space data.

The basic approach of retrospective motion correction relies on the Fourier properties. We will describe the correction for Cartesian *k*-space sampling but generalization to other sampling schemes is possible. As described above rigid body translational motion causes a linearly increasing phase shift in *k*-space. Knowing the translation in each direction Δx, Δy, and Δz, a phase correction $\Delta\varphi_{\mathrm{cor}}$ for each point in *k*-space can be applied to calculate the motion corrected *k*-space $S(k_x, k_y, k_z)_{\mathrm{cor}}$ (Bookwalter *et al* 2010):

$$S(k_x,k_y,k_z)_{cor}=S(k_x,k_y,k_z)_{orig}.\mathrm{e}^{-\mathrm{i}\Delta\phi_{cor}}=S(k_x,k_y,k_z)_{orig}.\mathrm{e}^{-\mathrm{i}2\pi(k_x\Delta x+k_y\Delta y+k_z\Delta z)}. \quad (3)$$

Since motion data are usually available per *k*-space line or set of *k*-space lines, the same phase correction is applied for a corresponding set of *k*-space points. This process is repeated for each *k*-space line in phase encoding direction (Ehman and Felmlee 1989, Hu and Kim 1994, Robson *et al* 1997, Mendes *et al* 2009, Bookwalter *et al* 2010, Vaillant *et al* 2014). For 2D imaging only in-plane translation can be corrected through this principle.

Rotation correction makes use of the Fourier rotation theorem (see figure 7). If $I(x,y,z)$ describes the image space and $S(k_x,k_y,k_z)$ is its Fourier transform (*k*-space), a rotation α in image space will result in the same rotation α in *k*-space with the rotation axis through the origin. Assuming a rotation around the *z*-axis in image space, the Fourier rotation theorem can be described as follows (Korin *et al* 1995):

$$I(x\,cos\,\alpha+y\,sin\,\alpha,-x\,sin\,\alpha+y\,cos\,\alpha,z)\supset S(k_x\,cos\,\alpha+k_y\,sin\,\alpha,-k_x\,sin\,\alpha+k_y\,cos\,\alpha,k_z). \quad (4)$$

A few practical issues have to be considered for rotational motion correction. First, an appropriate phase correction must be applied to ensure that the centre of rotation is at the centre of *k*-space (Korin *et al* 1995, Pipe 1999). Second, the correction scheme can produce 'pie-slice' regions of lower data point density in *k*-space where the Nyquist criterion may be violated. Data points in these regions may be estimated through, e.g. Partial Parallel Imaging (PPI) approaches (Aksoy *et al* 2006). The last major step is gridding of the data. The corrected *k*-space data do not necessarily lie on a rectilinear grid, which is necessary for fast Fourier transformation. Korin *et al* (1995) for instance used bilinear interpolation of the real and imaginary *k*-space data to solve this problem. However, an interpolation of non-Cartesian data to the Cartesian grid potentially results in blurred images (Forman *et al* 2011). Additional signal variations, e.g. due to spin history effects from through-plane motion, object parts that leave the field of view or deformable object motion cannot be considered in the described retrospective motion correction and cause residual artefacts. These may be minimized by reduced weighting of the affected *k*-space data during image reconstruction (Pipe 1999, Lin *et al* 2010).

4.2. Autofocusing

An entirely different class of correction methods is termed autofocusing and does not rely on motion information. These techniques therefore do not require specific data sampling, sequence design or hardware. The described approaches assume a rigid body or deformable object motion model and estimate the (few) motion model parameters by iterative optimization of an image quality metric when parts of the raw data are modified according to the motion model (Atkinson *et al* 1997).

Autofocusing methods apply estimated motion to lines or groups of lines in *k*-space until a cost function that represents image artefacts reaches its minimum. The correction is performed by iteratively applying the Fourier shift (equation (3)) and rotation theorem (equation (4)) to the *k*-space lines (Atkinson *et al* 1999). After inverse FFT, the resulting image quality is assessed using a cost function such as the image entropy (Atkinson *et al* 1997, Manduca *et al* 2000, Lin and Song 2006), the Gerchberg-Saxton algorithm (Hedley *et al* 1991) or the gradient entropy (Loktyushin *et al* 2013). It is assumed that once motion is estimated optimally, the cost function will be minimized resulting in a motion corrected image. These autofocusing techniques are computationally intensive and can potentially induce artefacts if motion is falsely estimated (McGee *et al* 2000a). More time-efficient approaches use additional motion information from navigator echoes (McGee *et al* 2000b), references images (Atkinson and Hill 2001) or self-navigation 'Butterfly' sequences (Cheng *et al* 2012) in a hybrid approach.

Retrospective motion correction techniques have the unique potential to compensate for deformable object motion (van Heeswijk *et al* 2012). The correction of this type of motion, however, requires an alternative approach resulting in a complex *k*-space model of translation, rotation, shearing, scaling or even more local types of motion. Batchelor *et al* (2005) presented one of the first methods to correct for deformable object motion. The corrected image is calculated by inversion of a general complex matrix equation expressing the motion corrupted image through the estimated motion model. The resulting image is evaluated by an image quality cost function. With higher complexity of the motion model, the estimation of more motion parameters is required and further increases the computational time (Cheng *et al* 2012). Atkinson *et al* (2006) and Liu *et al* (2005) expanded this method to diffusion imaging using additional navigator data reducing the number of unknown motion parameters in this hybrid approach.

5. Prospective motion correction

Prospective correction techniques perform a real-time update of the image acquisition. The goal of prospective motion correction (PMC) is to keep the acquisition field of view (FoV) constant relative to the moving object. This implies that the FoV can be adapted to the object pose by changing the gradient encoding and system RF settings. It is usually restricted to the correction of rigid body motion, e.g. of the head. An early approach to PMC was proposed by Haacke and Patrick (1986) where navigators monitored breathing motion and the phase encoding gradient was adapted to reduce artefacts from periodic 1D chest movement. In general, PMC applies motion detection techniques as discussed in chapter 3 and adapts the MRI pulse sequence during its run-time (often referred to as real-time). Obviously, motion tracking techniques for prospective motion correction need to deliver pose information frequently and fast enough. Accordingly PMC has employed 1D navigators (Lee *et al* 1996, Firmin and Keegan 2001, Norris and Driesel 2001, Weih *et al* 2004), orbital navigators (Fu *et al* 1995, Lee *et al* 1998, Ward *et al* 2000), spherical navigators (Welch *et al* 2002), cloverleaf navigators (van der Kouwe *et al* 2006), image based navigators (White *et al* 2010, Tisdall *et al* 2012), pickup-coils (‘active markers’) (Ooi *et al* 2009, 2011) or optical tracking systems (Speck *et al* 2006, Qin *et al* 2009, Andrews-Shigaki *et al* 2011). The application of motion information for prospective motion correction is shown in figure 8 and explained in the following sections.

5.1. Field of view positioning

To keep the FoV constant relative to a moving object, rotations can be corrected by adjusting the gradients such that the encoding field is kept constant for every point of the moving volume. This would also be possible for global object scaling and shearing by gradient amplitude scaling. However, the tracking device is usually limited to measure rigid body motion with 6 degrees of freedom (rotation and translation). To correct for translational motion, the centre frequency of the RF-pulses and of the receiver can be changed to shift the image in slice and read-out direction. To correct for translation in phase encoding direction, the receiver phase can be modulated during acquisition or shifted during reconstruction. A more detailed description of the required calculations is given, e.g. in Nehrke and Börnert (2005) or Zaitsev *et al* (2006).

5.2. Data delivery and sequence update

In PMC the acquisition process has to be informed about changes in pose or motion to allow and maintain the same FoV relative to the object via real-time updates. The transfer of motion data is strongly vendor specific and also depends on the method of pose detection. For example, the pose information can either come from the MR-system's image reconstruction and system internal real-time feedback mechanisms or from an external tracking system, e.g. via a network connection.

The initial position and orientation (pose) of the imaging volume is known and serves as the reference pose. During the scan only the differences between the current pose and its initial pose are required. The position and orientation of the imaging volume is then modified corresponding to these differences. The new imaging volume parameters are handed over to the scanner, which calculates the gradients and frequencies accordingly. The calculation requires time (typically milliseconds) and the updated gradient waveforms need to be transferred to the executing digital signal processor (DSP) before they can be applied. The procedure is soft- and hardware dependent but usually requires the identification of suitable periods within the sequence to insert the update mechanism.

Adjustments of the MR scanner's gradients and frequencies require the motion data in scanner coordinates. As described above, this may require the knowledge of a transformation matrix (which must be obtained via cross-calibration as described in section 3.3) to transform pose information from the external tracking device's into the scanner's coordinate system. For computational efficiency, motion correction implementations may use a quaternion representation (Zaitsev *et al* 2006) or homogeneous coordinates (Zahneisen and Ernst 2016) for coordinate and orientation calculations instead of an Euler angle description.

5.3. Latency and velocity of tracking systems

Commonly pose updates are performed per 'excitation' or 'per *k*-space line'. Depending on tracking frequency and sequence limitations, it can be necessary to reduce the update frequency to 'per slice' or 'per volume'. Intra-scan correction was proposed by Nehrke and Börnert (2005) if motion between excitation and readout becomes relevant. Herbst *et al* (2012, 2015) introduced prospective position updates between excitations and during the diffusion weighting period of a diffusion-weighted double spin echo segmented EPI sequence. Alternatively, to adapt the acquisition to the motion, the affected *k*-space line can be rejected and re-acquired if the motion is above a predefined threshold. However, this leads to increased scan time and is not always an option, e.g. in fMRI, where the time of the sequence is synchronized to other aspects of the experiment.

The latency of the entire system including pose detection, data transfer, gradient recalculation, and DSP update results in residual differences in the object to FoV relation. In addition, the time between sequence update and data acquisition determines further errors. According to Maclaren *et al* (2010) the accuracy of the tracking system should be five to ten times higher than the resolution of the data being acquired. The best implementations using external tracking systems such as described in (Andrews-Shigaki *et al* 2011, Maclaren *et al*

2012) have a latency of about 20–30 ms. Thus, for a resolution of 1.0 mm, velocities of about 3.0–10.0 mm s^{-1} would be acceptable.

For implementations using navigators, which are normally played out once per TR, the sequence timing and post processing should be designed carefully to minimize latency. One way to reduce latency effects is the use of predictive filtering. A Kalman filter (Maclaren *et al* 2009, 2011, White *et al* 2010) and predictor (Kalman 1960) were proposed for pose prediction. Data transfer and processing, however, might increase latency. Further correction for residual errors between prediction and true pose can be applied retrospectively when the pose data is fully available, e.g. by using a Kalman smoother (Maclaren *et al* 2009).

5.4. Advantages and limitations

Prospective motion correction proved to be a flexible tool that can be implemented into all MR sequences provided the MR system is capable of dynamic updates during the sequence run-time. In figure 9, two examples of motion-corrupted and motion-corrected brain images using an optical motion detection system are presented. They exemplify two main use cases, i.e. improvement of ‘good’ data to even better quality (mainly for research applications) and retrieval of otherwise non-diagnostic images. Most modern MR systems provide the required real-time feedback capabilities or interfaces to communicate with external devices. PMC has been demonstrated to be efficient in the prevention of motion artefacts originating from displacements between acquisition steps as well as sequence specific motion effects such as signal dropouts due to dephasing or misalignment of the encoding direction for diffusion or flow measurements. PMC also accounts for spin-history effects when through-plane motion otherwise causes the magnetization to enter or exit the excited imaging volume. Without PMC, this can lead to signal differences due to different saturation and relaxation. In addition, the intended *k*-space acquisition scheme is maintained and thus no unintended *k*-space density variations occur. Many of these disadvantageous effects, i.e. spin history, *k*-space sampling density, and dephasing effects cannot be corrected retrospectively.

As prospective motion correction adapts the sequence during runtime and ensures consistent *k*-space data, no additional calculation time is needed for the reconstruction making PMC attractive for real time MR applications. A prerequisite for successful PMC is the acquisition of reliable tracking data with high accuracy and precision. Noisy or inaccurate pose data can corrupt the image data and lead to artefacts. Reverting to uncorrected data is not possible. However, the corrected data may be ‘de-corrected’ by reverse retrospective reconstruction (Zahneisen *et al* 2015). Higher order effects such as changing $B0$ inhomogeneities and gradient imperfections cannot be corrected by PMC. They lead to a violation of the rigid body assumption. Combination with retrospective correction is possible and can address these issues partially (Boegle *et al* 2010, Maclaren *et al* 2011, Aksoy *et al* 2012).

6. Further considerations for motion correction

Inherent tracking precision and accuracy (Maclaren *et al* 2011) as well as delay between pose detection and sequence update can lead to residual artefacts that degrade correction data, in particular for large motion (Maclaren *et al* 2013). These artefacts cannot be

compensated if the rigid body assumption fails. These challenges include transmit and receive radiofrequency field inhomogeneity, gradient nonlinearity and $B0$ inhomogeneity.

6.1. Transmit field heterogeneity

The RF transmit field ($B1+$) is largely uniform at low field strength up to 1.5 T where a body coil is used for excitation. At higher field strengths the RF frequency for proton MRI increases leading to shorter wave length and inhomogeneous $B1+$ within tissue (Yang *et al* 2002). Local flip angle variations due to motion can result in inconsistent data with intensity variations between poses. The excitation field can be more homogeneous using parallel transmission technology (Katscher *et al* 2003, Setsompop *et al* 2006). However, dynamic measurements of $B1+$ field changes and adaptation of the respective parallel transmission settings is an ongoing challenge. Recently, the impact of motion on parallel transmission in finite difference time domain (FDTD) simulations for 7T was studied by Bammer *et al* (2011). The result showed that the transmit $B1+$ field strongly depends on the object pose within the coil. In addition, Bloch-simulated RF excitation patterns appeared less uniform for higher reduction factors ($R = 2$, 3, and 4) and stronger motion. This effect remains a challenge for prospective and retrospective motion correction.

6.2. Receive field heterogeneity

Multiple receiver coil arrays are commonly applied to yield higher signal-to-noise ratio (SNR) and allow accelerated image acquisition. When motion occurs in measurements with stationary multi-coil receive arrays, the coil sensitivities will change relative to the moving object. With PMC, the coil sensitivities effectively move relative to a stationary object. This results in variation of signal amplitude and phase, leading to shading artefacts after coil combination (Atkinson *et al* 2004, Banerjee *et al* 2013). Such artefacts appear more prominently in parallel imaging with high reduction factors and for arrays of small receiver coils with strong sensitivity profile variations in space. Bammer *et al* (2007) introduced a retrospective correction method to mitigate such artefacts and termed it augmented sensitivity encoding (augmented SENSE) reconstruction. The explicit determination of coil sensitivities for each motion pose, however, is still impractical and time consuming. Banerjee *et al* (2013) showed that the coil sensitivities for different poses can be generated by regridding the initial dataset followed by non-iterative reconstruction. Nevertheless, this may be inapplicable in iterative SENSE which is sensitive to errors in the model estimation, especially when the object moves outside the area of the initial sensitivity maps estimation. A fast pre-scan for generating the sensitivity maps prior to imaging may be a solution (Bammer *et al* 2007). Yarach *et al* (2015b) showed that varying coil sensitivities can be determined from repeated central k-space sampling.

6.3. Gradient nonlinearity

In stationary MR imaging, gradient nonlinearity (GNL) effects are seen as warping (geometric distortions) of the object particularly at the edges of large FoVs, which can be corrected since the gradient field distribution is known. Unlike in static imaging, motion during the acquisition with GNL leads to blurring in addition to spatial distortion because imaging data acquired at multiple object locations within the non-linear gradient fields have different geometry. Thus, the k-space data of the object become inconsistent between phase

encoding steps. This effect is again strongest in peripheral regions (Polzin *et al* 2004, Hu *et al* 2005). For head imaging Yarach *et al* (2015a) showed that this effect is less relevant than coil sensitivity variations. This effect depends strongly on the object size and gradient type (Wang *et al* 2004, Doran *et al* 2005, Baldwin *et al* 2007). However, it is relevant for larger motion and can also be corrected using an extension of the iterative augmented SENSE reconstruction. Since the gradient nonlinearity is known for a given gradient coil no additional measurements or estimations are necessary. GNL leads to three types of distortion in 2D image acquisitions (Sumanaweera *et al* 1994) which include barrel, potato chip, and bow-tie effects, each named after the shape of slice distortion. Only the barrel effect occurs in 3D acquisitions where a weak or no slice selection gradient is applied (Walton *et al* 1997). The barrel effect is deterministic, so it can be mathematically corrected for 3D datasets (Sumanaweera *et al* 1994, Yarach *et al* 2015a). Variations of the 2D slice selection distortion due to motion cause inconsistencies in single slice *k*-space data which require a different approach for correction and still remain a challenge.

6.4. B0 inhomogeneity

Even if real-time pose correction of the imaging volume is performed very accurately, motion-induced magnetic field changes may occur due to the main magnetic field inhomogeneity and object induced field changes. These local magnetic field changes are frequently considered as the main source of residual artefacts. They are most prominent in EPI, which is very sensitive to field inhomogeneity due to the low effective phase-encoding bandwidth (Jezzard and Balaban 1995, Jezzard and Clare 1999). Recently, the size and location of $B0$ field shifts within the brain at 7T for different types of head movement were studied by Sulikowska *et al* (2014). Their results showed that for pitch rotation, the $B0$ field variation was (-1.32 ± 0.2) Hz/ degree and (-1.00 ± 0.09) Hz/degree in the centre of the frontal and occipital lobes, respectively. Other authors have reported maximum $B0$ field differences caused by head movement of 160 Hz at 2.89 T (Zhou *et al* 1998) and 50 Hz at 3T (Jezzard and Clare 1999). Field changes cause two effects: geometric distortions and signal dropouts. If known, these static geometric distortions can be considered in the reconstruction using the pixel shift method (Jezzard and Balaban 1995) and can be corrected in the presence of motion as described above. Several techniques for dynamic $B0$ field mapping have been proposed including dual echo-time field mapping (Reber *et al* 1998, Hutton *et al* 2002), reference maps calculated using Fourier methods (Chen and Wyrwicz 1999, 2001), point spread function mapping (Zeng and Constable 2002), and reversed gradient polarities (Andersson *et al* 2003). However, they require additional scan time and assume that the subject remains still for each measurement step. For faster motion, the distortion caused by $B0$ field inhomogeneity has been tackled for single-shot EPI time series where each acquisition provides a field map (Sutton *et al* 2004, Splitthoff and Zaitsev 2009, Boegle *et al* 2010, Ooi *et al* 2013a). Extension to multi-short EPI and other spin-warp sequences is not obvious. In fact, even if the field maps can be determined for each motion pose, local signal variation due to changing field homogeneity (T2* variation) cannot be recovered retrospectively. Figure 10 demonstrates that the motion-induced field inhomogeneities lead to severe signal dropouts, particularly at the air-tissue interfaces.

A prospective solution may be dynamic shimming during imaging. Typically, modern scanners have a set of room temperature shim coils consisting of the three linear gradients and five second order shims (Clare *et al* 2006). These coils produce magnetic fields based on the spherical harmonic series to correct low order spatial perturbations. The current in these coils may be updated concurrently with object movement. Again, dynamic field information is required. Ward *et al* (2002) introduced real-time auto shimming using a navigator pulse sequence (shim NAV) to acquire field information for updating the first order shim-compensated EPI acquisition in the presence of subject motion. A 3D EPI navigator (Hess *et al* 2011) was also employed to achieve simultaneous motion and shim correction in single voxel MR Spectroscopy. Keating *et al* (2012) showed that fast $B0$ mapping for an MRS voxel (20 mm × 20 mm × 11.7 mm) can be performed in approximately 120 ms. In addition, knowing the higher than first order dynamic field fluctuations around the head may be helpful. These fluctuations may be monitored by field cameras (Barmet *et al* 2008) concurrently with image acquisition. Information about these global field changes and appropriate updates of the higher order shim currents (Duerst *et al* 2014) may allow minimizing the field fluctuation-induced artefacts in motion correction. The combination of these methods with prospective motion correction has not been reported but is generally feasible.

7. Conclusion

Motion in MRI is a relevant problem. Without motion correction techniques the sensitivity to motion during conventional image acquisition results in unavoidable artefacts, which can reduce the image quality, diagnostic, and scientific information content. Motion artefacts can appear as ghosting, blurring, and geometric distortion or apparently decreased SNR. Variations in the magnetization caused by material or tissue susceptibilities lead to displacement and blurring. Consequently, the full nominal resolution of MRI is often not realized leading to loss of potential information in research studies even if the imaging data are not visually corrupted. The application of prospective motion correction methods to highest resolution *in vivo* MR brain imaging at 7T has demonstrated the possibility to acquire imaging data with resolution down to 120 micrometer in human subjects (Stucht *et al* 2015). In clinical diagnostic applications of MRI, subject motion frequently leads to imaging data of such low quality that they can become non-diagnostic in up to 30% of all patients and require repeated examinations that increase imaging costs (Andre *et al* 2015).

Motion artefacts strongly depend on the type of motion and the acquisition strategy. This led to a large variety of techniques for the reduction or correction of motion artefacts which can be classified in retrospective and prospective approaches. However, many correction methods are only applicable for specific motion patterns or imaging sequences. Until now, no single technique was demonstrated to fully correct any motion-induced artefact, in particular for fast and irregular motion of large amplitude. Using the appropriate motion correction technique, however, can improve the MR image quality dramatically. For diagnostic purposes, the images do not necessarily need to be artefact-free but non-diagnostic imaging data has to be improved to reliably diagnose relevant disease. In research applications that aim at higher image resolution, e.g. in an UHF environment, best image

quality requires correction of even very small and unavoidable motion such as motion caused by heart beat or breathing.

In order to apply an appropriate motion correction the object motion has to be known or estimated. Several detection techniques exist which can determine motion of up to 6 degrees of freedom assuming rigid body motion and up to 12 degrees of freedom for deformable object motion. A suitable detection strategy has to be chosen depending on the required precision, latency, and accuracy of the motion correction together with the timing constraints of the acquisition method. For example, prospective correction techniques require a system with low latency whereas in retrospective correction the latency is of minor importance as long as it is known. Furthermore, novel techniques aim to remove the residual artefacts and distortions due to gradient field nonlinearity as well as $B0$ field inhomogeneities that occur even in perfectly motion corrected data. A generic motion correction solution that can be applied to any MR acquisition method without changes in sequence timing or reconstruction, such as external tracking with prospective correction, requires additional hardware and system integration efforts. Many of these correction techniques have shown to be very effective in reducing motion artefacts but most methods did not leave the research laboratories yet and are thus not available on clinical MRI systems. Other methods that can be well integrated into existing MRI systems by sequence modifications without requiring additional hardware, such as PROPELLER or PROMO, are commercially available but can correct motion in only very few specific imaging methods and assume little intra-scan motion. It is not yet clear which of the concepts will be broadly applied in future generations of MRI systems. As of today, only few motion correction techniques found their way into the clinical routine and motion prevention is still most commonly used to reduce motion artefacts. External motion tracking hardware adds costs and technical complexity in system integration and operation and may be an obstacle for broader market introduction.

Only few studies have addressed the prevalence and clinical or financial consequences of subject motion in MRI (Andre *et al* 2015). In addition, no large systematic studies have proven the effectiveness, clinical or financial benefits of motion correction in MRI. As motion correction methods are becoming available, such studies are indicated to pave the way towards wider distribution and acceptance for the benefit of the patient and the health care system.

Acknowledgments

The work of this paper is partly funded by the Federal Ministry of Education and Research within the Forschungscampus STIMULATE under grant number ‘13GW0095A’, the FP7 Marie Curie Actions of the European Commission (FP7-PEOPLE-2012-ITN-316716) and NIH grant R01DA021146.

References

Ackerman, J., et al. Rapid 3D tracking of small RF coils. Proc 5th Annual Meeting of ISMRM; Montréal, Canada. 1986. p. 1131-2.

Aksoy M. Real time prospective motion—correction ii—practical solutions. Current Concepts of Motion Correction for MRI & MRS; ISMRM Workshop Series. 2010

Aksoy, M., et al. A self-navigated spiral in and out pulse sequence design for retrospective motion correction. Proc 14th Scientific Meeting of ISMRM; 2006. p. 3197

Aksoy M, et al. Hybrid prospective and retrospective head motion correction to mitigate cross-calibration errors. Magn Reson Med. 2012; 67:1237–51. [PubMed: 21826729]

Anderson AW, Gore JC. Analysis and correction of motion artifacts in diffusion weighted imaging. Magn Reson Med. 1994; 32:379–87. [PubMed: 7984070]

Andersson JLR, Skare S, Ashburner J. How to correct susceptibility distortions in spin-echo echo-planar images: application to diffusion tensor imaging. NeuroImage. 2003; 20:870–88. [PubMed: 14568458]

Anderson, AG., et al. Retrospective registration-based MRI motion correction with interleaved radial trajectories. Proc.—Int Symp on Biomedical Imaging; 2011. p. 1528-31.

Andre JB, et al. Toward quantifying the prevalence, severity, and cost associated with patient motion during clinical MR examinations. J Am Coll Radiol. 2015; 12:689–95. [PubMed: 25963225]

Andrews-Shigaki BC. Prospective motion correction for magnetic resonance spectroscopy using single camera retro-grate reflector optical tracking. J Magn Reson Imag. 2011; 33:498–504.

Atkinson, D.; Hill, DLG. Automatic motion correction using prior knowledge. Proc 9th Annual Meeting ISMRM; 2001. p. 747

Atkinson D, et al. Automatic correction of motion artifacts in magnetic resonance images using an entropy focus criterion. IEEE Trans Med Imag. 1997; 16:903–10.

Atkinson D, et al. Automatic compensation of motion artifacts in MRI. Magn Reson Med. 1999; 41:163–70. [PubMed: 10025625]

Atkinson D, et al. Coil-based artifact reduction. Magn Reson Med. 2004; 52:825–30. [PubMed: 15389945]

Atkinson D, et al. Nonlinear phase correction of navigated multi-coil diffusion images. Magn Reson Med. 2006; 56:1135–9. [PubMed: 16986111]

Baldwin LN. Characterization, prediction, and correction of geometric distortion in 3 T MR images. Med Phys. 2007; 34:388–99. [PubMed: 17388155]

Bammer R, Aksoy M, Liu C. Augmented generalized SENSE reconstruction to correct for rigid body motion. Magn Reson Med. 2007; 57:90–102. [PubMed: 17191225]

Bammer, R., et al. Impact of motion on parallel transmission. Proc 19th Scientific Meeting ISMRM; 2011. p. 4590

Banerjee S, et al. Parallel and partial Fourier imaging with prospective motion correction. Magn Reson Med. 2013; 69:421–33. [PubMed: 22488750]

Barmet C, De Zanche N, Pruessmann KP. Spatiotemporal magnetic field monitoring for MR. Magn Reson Med. 2008; 60:187–97. [PubMed: 18581361]

Batchelor PG, et al. Matrix description of general motion correction applied to multishot images. Magn Reson Med. 2005; 54:1273–80. [PubMed: 16155887]

Bernstein, MA.; King, KF.; Zhou, XJ. Handbook of MRI Pulse Sequences. Amsterdam: Elsevier; 2004.

Bertelsen, A., et al. Tractography in the fetal brain with correction of fetal and maternal motion using model-based slice to volume registration. Proc. 17th Scientfic Meeting ISMRM; 2009. p. 3416

Boegle R, Maclaren J, Zaitsev M. Combining prospective motion correction and distortion correction for EPI: towards a comprehensive correction of motion and susceptibility-induced artifacts. Magn Reson Mater Phys Biol Med. 2010; 23:263–73.

Bookwalter CA, Griswold MA, Duerk JL. Multiple overlapping *k*-space junctions for investigating translating objects (MOJITO). IEEE Trans Med Imag. 2010; 29:339–49.

Boussel L, et al. Swallowing, arterial pulsation, and breathing induce motion artifacts in carotid artery MRI. J Magn Reson Imag. 2006; 23:413–5.

Butts K, et al. Diffusion-weighted interleaved echo-planar imaging with a pair of orthogonal navigator echoes. Magn Reson Med. 1996; 35:763–70. [PubMed: 8722828]

Bydder M, Larkman DJ, Hajnal JV. Detection and elimination of motion artifacts by regeneration of *k*-space. Magn Reson Med. 2002; 47:677–86. [PubMed: 11948728]

Chen NK, Wyrwicz AM. Correction for EPI distortions using multi-echo gradient-echo imaging. Magn Reson Med. 1999; 41:1206–13. [PubMed: 10371453]

Chen NK, Wyrwicz AM. Optimized distortion correction technique for echo planar imaging. Magn Reson Med. 2001; 45:525–8. [PubMed: 11241714]

Cheng JY, et al. Nonrigid motion correction in 3D using autofocusing with localized linear translations. Magn Reson Med. 2012; 68:1785–97. [PubMed: 22307933]

Clare S, Evans J, Jezzard P. Requirements for room temperature shimming of the human brain. Magn Reson Med. 2006; 55:210–4. [PubMed: 16315227]

de Crespigny AJ, et al. Navigated diffusion imaging of normal and ischemic human brain. Magn Reson Med. 1995; 33:720–8. [PubMed: 7596277]

Derbyshire JA, et al. Dynamic scan-plane tracking using MR position monitoring. J Magn Reson Imag. 1998; 8:924–32.

Doran SJ, et al. A complete distortion correction for MR images: I. Gradient warp correction. Phys Med Biol. 2005; 50:1343–61. [PubMed: 15798328]

Duerst Y, et al. Real-time feedback for spatiotemporal field stabilization in MR systems. Magn Reson Med. 2014; 73:884–93. [PubMed: 24634192]

Dumoulin CL, Souza SP, Darrow RD. Real-time position monitoring of invasive devices using magnetic resonance. Magn Reson Med. 1993; 29:411–5. [PubMed: 8450752]

Ehman RL, Felmlee JP. Adaptive technique for high-definition MR imaging of moving structures. Radiology. 1989; 173:255–63. [PubMed: 2781017]

Firmin D, Keegan J. Navigator echoes in cardiac magnetic resonance. J Cardiovasc Magn Reson. 2001; 3:183–93. [PubMed: 11816615]

Forman C, et al. Self-encoded marker for optical prospective head motion correction in MRI. Med Image Anal. 2011; 15:708–19. [PubMed: 21708477]

Fu ZW, et al. Orbital navigator echoes for motion measurements in magnetic resonance imaging. Magn Reson Med. 1995; 34:746–53. [PubMed: 8544696]

Gai N, Axel L. Correction of motion artifacts in linogram and projection reconstruction MRI using geometry and consistency constraints. Med Phys. 1996; 23:251–62. [PubMed: 8668107]

Haacke EM, Patrick JL. Reducing motion artifacts in two-dimensional Fourier transform imaging. Magn Reson Imag. 1986; 4:359–76.

Hedley M, Yan H, Rosenfeld D. Motion artifact correction in MRI using generalized projections. IEEE Trans Med Imag. 1991; 10:40–6.

Heiland S. From A as in aliasing to Z as in zipper: artifacts in MRI. Clin Neuroradiol. 2008; 18:25–36.

Hennig J. *K*-space sampling strategies. Eur Radiol. 1999; 9:1020–31. [PubMed: 10415232]

Herbst M, et al. Prospective motion correction with continuous gradient updates in diffusion weighted imaging. Magn Reson Med. 2012; 67:326–38. [PubMed: 22161984]

Herbst M, et al. Prospective motion correction of segmented diffusion weighted EPI. Magn Reson Med. 2015; 4:1675–81. [PubMed: 25446934]

Hess AT, et al. Real-time motion and *B*0 corrected single voxel spectroscopy using volumetric navigators. Magn Reson Med. 2011; 66:314–23. [PubMed: 21381101]

Hu HH, et al. Continuously moving table MRI with SENSE: application in peripheral contrast enhanced MR angiography. Magn Reson Med. 2005; 54:1025–31. [PubMed: 16149061]

Hu X, Kim SG. Reduction of signal fluctuation in functional MRI using navigator echoes. Magn Reson Med. 1994; 31:495–503. [PubMed: 8015402]

Huizinga, W., et al. Groupwise registration for correcting subject motion and eddy current distortions in diffusion MRI using a PCA based dissimilarity metric. In: Schultz, T., et al., editors. MICCAI Workshop on Computational Diffusion MRI and Brain Connectivity; Berlin: Springer; 2014. p. 163-74.

Hutton C, et al. Image distortion correction in fMRI: a quantitative evaluation. NeuroImage. 2002; 16:217–40. [PubMed: 11969330]

Jenkinson M, et al. Improved optimization for the robust and accurate linear registration and motion correction of brain images. NeuroImage. 2002; 17:825–41. [PubMed: 12377157]

Jenkinson M, Smith S. A global optimisation method for robust affine registration of brain images. Med Image Anal. 2001; 5:143–56. [PubMed: 11516708]

Jezzard P, Balaban RS. Correction for geometric distortion in echo-planar images from B-0 field variations. Magn Reson Med. 1995; 34:65–73. [PubMed: 7674900]

Jezzard P, Clare S. Sources of distortion in functional MRI data. Human Brain Mapp. 1999; 8:80–5.

Jiang A, et al. Motion detection and correction in functional MR imaging. Human Brain Mapp. 1995; 3:224–35.

Kadashevich I, Danishad A, Speck O. Automatic motion selection in one step cross-calibration for prospective MR motion correction. Magn Reson Mater Phys Biol Med. 2011; 24:266–7.

Kalman RE. A new approach to linear filtering and prediction problems. Trans ASME—J Basic Eng. 1960; 82:35–45.

Katscher U, et al. Transmit SENSE. Magn Reson Med. 2003; 49:144–50. [PubMed: 12509830]

Keating B, Ernst T. Real-time dynamic frequency and shim correction for single-voxel magnetic resonance spectroscopy. Magn Reson Med. 2012; 68:1339–45. [PubMed: 22851160]

Kim B, et al. Motion correction in fMRI via registration of individual slices into an anatomical volume. Magn Reson Med. 1999; 41:964–72. [PubMed: 10332880]

Kim K, et al. Intersection based motion correction of multislice MRI for 3-D in utero fetal brain image formation. IEEE Trans Med Imag. 2010; 29:146–58.

Kober T, et al. Head motion detection using FID navigators. Magn Reson Med. 2011; 66:135–43. [PubMed: 21337424]

Kochunov P, et al. Retrospective motion correction protocol for high-resolution anatomical MRI. Human Brain Mapp. 2006; 27:957–62.

Korin HW, et al. Spatial-frequency-tuned markers and adaptive correction for rotational motion. Magn Reson Med. 1995; 33:663–9. [PubMed: 7596270]

Krueger, S., et al. Prospective intra-image compensation for non-periodic rigid body motion using active markers. Proc 14th Scientific Meeting ISMRM; 2006. p. 3196

Lauzon ML, Rutt BK. Generalized *K*-space analysis and correction of motion effects in MR imaging. Magn Reson Med. 1993; 30:438–46. [PubMed: 8255191]

Lee CC, et al. Real-time adaptive motion correction in functional MRI. Magn Reson Med. 1996; 36:436–44. [PubMed: 8875415]

Lee CC, et al. A prospective approach to correct for inter-image head rotation in fMRI. Magn Reson Med. 1998; 39:234–43. [PubMed: 9469706]

Lin W, Song HK. Improved optimization strategies for autofocusing motion compensation in MRI via the analysis of image metric maps. Magn Reson Imag. 2006; 24:751–60.

Lin W, et al. Motion correction using an enhanced floating navigator and GRAPPA operations. Magn Reson Med. 2010; 63:339–48. [PubMed: 19918907]

Liu C, Moseley ME, Bammer R. Simultaneous phase correction and SENSE reconstruction for navigated multi-shot DWI with non-cartesian *k*-space sampling. Magn Reson Med. 2005; 54:1412–22. [PubMed: 16276497]

Liu C, et al. Self-navigated interleaved spiral (SNAILS): application to high-resolution diffusion tensor imaging. Magn Reson Med. 2004; 52:1388–96. [PubMed: 15562493]

Loktyushin A, et al. Blind retrospective motion correction of MR images. Magn Reson Med. 2013; 70:1608–18. [PubMed: 23401078]

Maclaren, J., et al. A Kalman filtering framework for prospective motion correction. Proc 17th Scientific Meeting ISMRM; 2009. p. 4602

Maclaren J, et al. Navigator accuracy requirements for prospective motion correction. Magn Reson Med. 2010; 63:162–70. [PubMed: 19918892]

Maclaren J, et al. Combined prospective and retrospective motion correction to relax navigator requirements. Magn Reson Med. 2011; 65:1724–32. [PubMed: 21590805]

Maclaren J, et al. Measurement and correction of microscopic head motion during magnetic resonance imaging of the brain. PLoS One. 2012; 7:e48088. [PubMed: 23144848]

Maclaren J, et al. Prospective motion correction in brain imaging: a review. Magn Reson Med. 2013; 69:621–36. [PubMed: 22570274]

Manduca A, et al. Autocorrection in MR imaging: adaptive motion correction without navigator echoes. Radiology. 2000; 215:904–9. [PubMed: 10831720]

Mangin JF, et al. Distortion correction and robust tensor estimation for MR diffusion imaging. Med Image Anal. 2002; 6:191–8. [PubMed: 12270226]

Marsland S, Twining CJ, Taylor CJ. A minimum description length objective function for groupwise non-rigid image registration. Image Vision Comput. 2008; 26:333–46.

McGee KP, et al. Image metric-based correction (autocorrection) of motion effects: analysis of image metrics. J Magn Reson Imag. 2000a; 11:174–81.

McGee KP, et al. Rapid autocorrection using prescan navigator echoes. Magn Reson Med. 2000b; 43:583–8. [PubMed: 10748434]

Mendes J, Kholmovski E, Parker DL. Rigid-body motion correction with self-navigation MRI. Magn Reson Med. 2009; 61:739–47. [PubMed: 19097240]

Metz CT, et al. Nonrigid registration of dynamic medical imaging data using *n*D + t B-splines and a groupwise optimization approach. Med Image Anal. 2011; 15:238–49. [PubMed: 21075672]

Miller, EG.; Matsakis, NE.; Viola, PA. Learning from one example through shared densities on transforms. Proc IEEE Conf on Computer Vision and Pattern Recognition; 2000. p. 464-71.

Nehrke K, Börnert P. Prospective correction of affine motion for arbitrary MR sequences on a clinical scanner. Magn Reson Med. 2005; 54:1130–8. [PubMed: 16200564]

Norris DG, Driesel W. Online motion correction for diffusion-weighted imaging using navigator echoes: application to RARE imaging without sensitivity loss. Magn Reson Med. 2001; 45:729–33. [PubMed: 11323797]

Ooi MB, et al. Prospective real-time correction for arbitrary head motion using active markers. Magn Reson Med. 2009; 62:943–54. [PubMed: 19488989]

Ooi MB, et al. Echo-planar imaging with prospective slice-by-slice motion correction using active markers. Magn Reson Med. 2011; 66:73–81. [PubMed: 21695720]

Ooi MB, et al. Combined prospective and retrospective correction to reduce motion-induced image misalignment and geometric distortions in EPI. Magn Reson Med. 2013a; 69:803–11. [PubMed: 22499027]

Ooi MB, et al. Prospective motion correction using inductively coupled wireless RF coils. Magn Reson Med. 2013b; 70:639–47. [PubMed: 23813444]

Ordidge RJ, et al. Correction of motional artifacts in diffusion-weighted MR images using navigator echoes. Magn Reson Imag. 1994; 12:455–60.

Paschal CB, Morris HD. *K*-space in the clinic. J Magn Reson Imag. 2004; 19:145–59.

Pipe JG. Motion correction with PROPELLER MRI: application to head motion and free-breathing cardiac imaging. Magn Reson Med. 1999; 42:963–9. [PubMed: 10542356]

Polzin JA, et al. Correction for gradient nonlinearity in continuously moving table MR imaging. Magn Reson Med. 2004; 52:181–7. [PubMed: 15236384]

Qin L, et al. Prospective head-movement correction for high-resolution MRI using an in-bore optical tracking system. Magn Reson Med. 2009; 62:924–34. [PubMed: 19526503]

Qin L, et al. Prospective motion correction using tracking coils. Magn Reson Med. 2013; 69:749–59. [PubMed: 22565377]

Reber PJ, et al. Correction of off resonance-related distortion in echo-planar imaging using EPI-based field maps. Magn Reson Med. 1998; 39:328–30. [PubMed: 9469719]

Robson MD, Anderson AW, Gore JC. Diffusion-weighted multiple shot echo planar imaging of humans without navigation. Magn Reson Med. 1997; 38:82–8. [PubMed: 9211383]

Rousseau F, et al. A novel approach to high resolution fetal brain MR imaging. Med Image Comput Comput-Assist Intervention. 2005; 8:548–55.

Schulz J, et al. An embedded optical tracking system for motion-corrected magnetic resonance imaging at 7 T. Magn Reson Mater Phys Biol Med. 2012; 25:443–53.

Sengupta S, et al. Prospective real-time head motion correction using inductively coupled wireless NMR probes. Magn Reson Med. 2013; 72:971–85. [PubMed: 24243810]

Setsompop K, et al. Parallel RF transmission with eight channels at 3 tesla. Magn Reson Med. 2006; 56:1163–71. [PubMed: 17036289]

Shankaranarayanan A, et al. Two-step navigatorless correction algorithm for radial *k*-space MRI acquisitions. Magn Reson Med. 2001; 45:277–88. [PubMed: 11180436]

Shechter, G.; McVeigh, ER. MR motion correction of 3D affine deformations. Proc 11th Scientific Meeting of ISMRM; 2003. p. 1054

Singh A, et al. Optical tracking with two markers for robust prospective motion correction for brain imaging. Magn Reson Mater Phys Biol Med. 2015; 28:523–34.

Speck O, Hennig J, Zaitsev M. Prospective real-time slice-by-slice motion correction for fMRI in freely moving subjects. Magn Reson Mater Phys Biol Med. 2006; 19:55–61.

Splitthoff DN, Zaitsev M. SENSE shimming (SSH): a fast approach for determining *B*0 field inhomogeneities using sensitivity coding. Magn Reson Med. 2009; 62:1319–25. [PubMed: 19780179]

Stucht D, et al. Highest resolution *in vivo* human brain MRI using prospective motion rcorrection. PLoS One. 2015; 10:e0133921. [PubMed: 26226146]

Studholme C. Mapping fetal brain development in utero using magnetic resonance imaging: the Big Bang of brain mapping. Annu Rev Biomed Eng. 2011; 13:345–68. [PubMed: 21568716]

Sulikowska, A., et al. Will field shifts due to head rotation compromise motion correction?. Proc 22nd Scientific Meeting of ISMRM; 2014. p. 885

Sumanaweera TS, et al. Characterization of spatial distortion in magnetic resonance imaging and its implications for stereotactic surgery. Neurosurgery. 1994; 35:696–704. [PubMed: 7808613]

Sutton BP, Noll DC, Fessler JA. Dynamic field map estimation using a spiral-in/spiral-out acquisition. Magn Reson Med. 2004; 51:1194–204. [PubMed: 15170840]

Thesen S, et al. Prospective Acquisition Correction for head motion with image-based tracking for real-time fMRI. Magn Reson Med. 2000; 44:457–65. [PubMed: 10975899]

Tisdall MD, et al. Volumetric navigators for prospective motion correction and selective reacquisition in neuroanatomical MRI. Magn Reson Med. 2012; 68:389–99. [PubMed: 22213578]

Tremblay M, Tam F, Graham SJ. Retrospective coregistration of functional magnetic resonance imaging data using external monitoring. Magn Reson Med. 2005; 53:141–9. [PubMed: 15690513]

Umeyama S. Least-squares estimation of transformation parameters between two point patterns. IEEE Trans Pattern Anal Mach Intell. 1991; 13:376–80.

Vaillant G, et al. Retrospective rigid motion correction in *k*-space for segmented radial MRI. IEEE Trans Med Imag. 2014; 33:1–10.

van Heeswijk R, et al. Motion compensation strategies in magnetic resonance imaging. Crit Rev Biomed Eng. 2012; 40:99–119. [PubMed: 22668237]

van der Kouwe AJW, Benner T, Dale AM. Real-time rigid body motion correction and shimming using cloverleaf navigators. Magn Reson Med. 2006; 56:1019–32. [PubMed: 17029223]

van der Kouwe AJW, Dale AM. Real-time motion correction using octant navigators. Neuroimage. 2001; 13:48.

van der Kouwe, A., et al. Real-time prospective rigid-body motion correction with the EndoScout gradient-based tracking system. Proc 17th Scientific Meeting ISMRM; 2009. p. 4623

Wachinger C, Navab N. Simultaneous registration of multiple images: similarity metrics and efficient optimization. IEEE Trans Pattern Anal Mach Intell. 2013; 35:1221–33. [PubMed: 23520261]

Walton L, et al. Stereotactic localization with magnetic resonance imaging: a phantom study to compare the accuracy obtained using two-dimensional and three-dimensional data acquisitions. Neurosurgery. 1997; 41:131–7. [PubMed: 9218305]

Wang D, et al. Geometric distortion in clinical MRI systems: I. Evaluation using a 3D phantom. Magn Reson Imag. 2004; 22:1211–21.

Ward HA, et al. Prospective multiaxial motion correction for fMRI. Magn Reson Med. 2000; 43:459–69. [PubMed: 10725890]

Ward HA, Riederer SJ, Jack CR. Real-time autoshimming for echo planar timecourse imaging. Magn Reson Med. 2002; 48:771–80. [PubMed: 12417991]

Weih KS, et al. Online motion correction for diffusion-weighted segmented-EPI and FLASH imaging. Magn Reson Mater Phys Biol Med. 2004; 16:277–83.

Welch EB, et al. Spherical navigator echoes for full 3D rigid body motion measurement in MRI. Magn Reson Med. 2002; 47:32–41. [PubMed: 11754440]

Welch EB, et al. Self-navigated motion correction using moments of spatial projections in radial MRI. Magn Reson Med. 2004; 52:337–45. [PubMed: 15282816]

White N, et al. PROMO: real-time prospective motion correction in MRI using image-based tracking. Magn Reson Med. 2010; 63:91–105. [PubMed: 20027635]

Yang QX, et al. Analysis of wave behavior in lossy dielectric samples at high field. Magn Reson Med. 2002; 47:982–9. [PubMed: 11979578]

Yarach U, et al. Correction of gradient nonlinearity artifacts in prospective motion correction for 7 T MRI. Magn Reson Med. 2015a; 73:1562–9. [PubMed: 24798889]

Yarach, U., et al. The correction of motion-induced coil sensitivity miscalibration in parallel imaging with prospective motion correction. Proc 23rd Scientific Meeting, Int Society for Magnetic Resonance in Medicine; 2015b. p. 2558

Zahneisen B, et al. Fast noniterative calibration of an external motion tracking device. Magn Reson Med. 2014; 71:1489–500. [PubMed: 23788117]

Zahneisen B, et al. Reverse retrospective motion correction. Magn Reson Med. 2015; doi: 10.1002/mrm.25830

Zahneisen B, Ernst T. Homogeneous coordinates in motion correction. Magn Reson Med. 2016; 5:274–9. [PubMed: 25648318]

Zaitsev M, Maclaren J, Herbst M. Motion artifacts in MRI: a complex problem with many partial solutions. J Magn Reson Imag. 2015; 2:881–901.

Zaitsev M, et al. Magnetic resonance imaging of freely moving objects: prospective real-time motion correction using an external optical motion tracking system. Neuroimage. 2006; 31:1038–50. [PubMed: 16600642]

Zeng H, Constable RT. Image distortion correction in EPI: comparison of field mapping with point spread function mapping. Magn Reson Med. 2002; 48:137–46. [PubMed: 12111941]

Zhou XJ, et al. Concomitant magnetic-field-induced artifacts in axial echo planar imaging. Magn Reson Med. 1998; 39:596–605. [PubMed: 9543422]

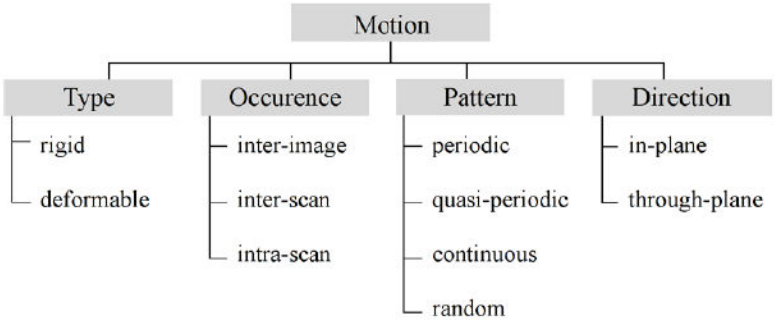

Figure 1.
Categories of motion correction.

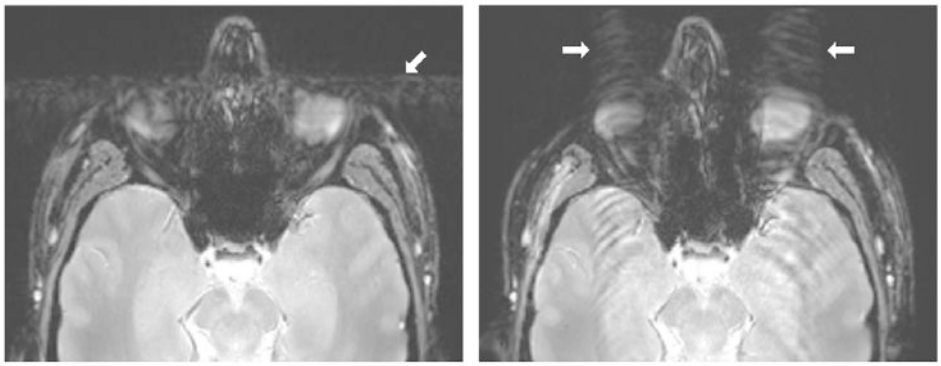

Figure 2.
In Cartesian MRI, motion artefacts mainly occur in phase direction. Eye movement with (a) horizontal and (b) vertical phase direction.

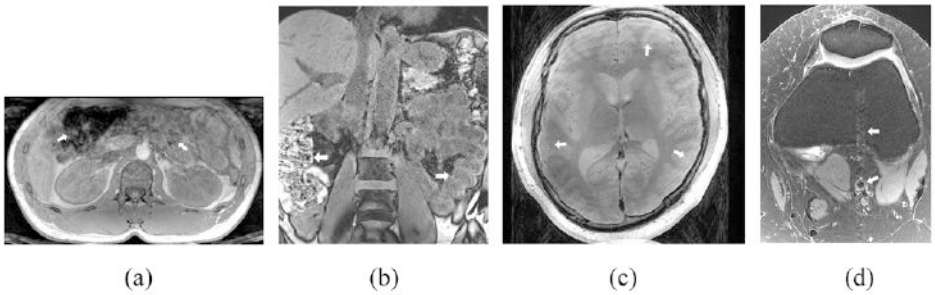

Figure 3.

Motion artefacts depending on motion pattern and direction with (a) periodic respiratory motion, (b) peristaltic motion, and random motion patterns with (c) in-plane head motion, and (d) through-plane flow motion.

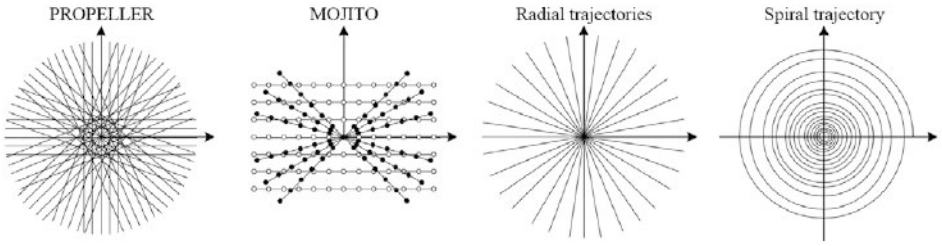

Figure 4.
K-space trajectories used in the different self-navigation techniques.

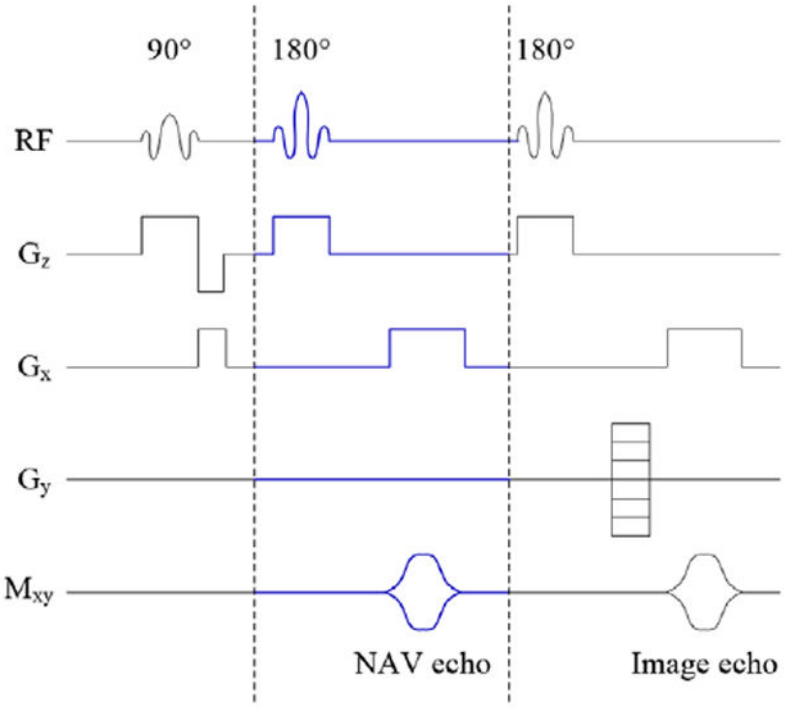

Figure 5.
Spin-echo sequence with additional linear NAV echo acquisition (between dotted lines) as proposed in (Ehman and Felmlee 1989).

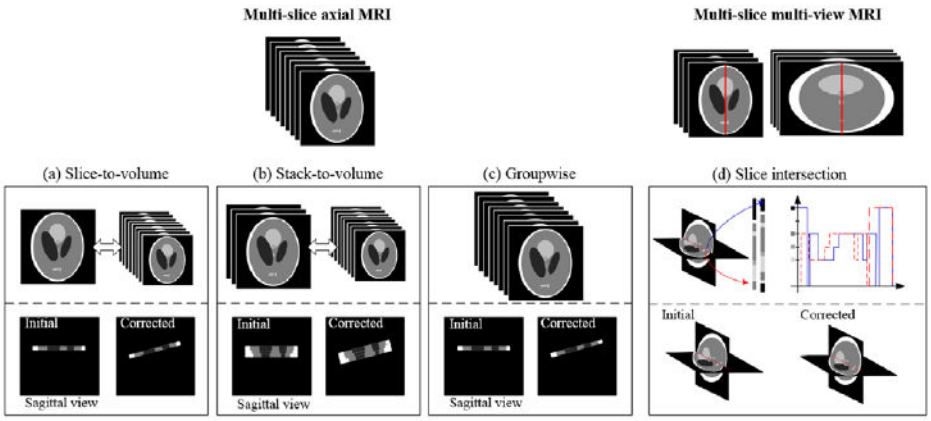

Figure 6.

Motion tracking using image registration. Acquiring multi-slice axial MRI data sets, the motion can be measured as (a) slice-to-volume, (b) stack-to-volume, and (c) group-wise approach. The slice intersection technique can be applied, when multi-slice multi-view (coronal, transversal, sagittal) acquisition is used.

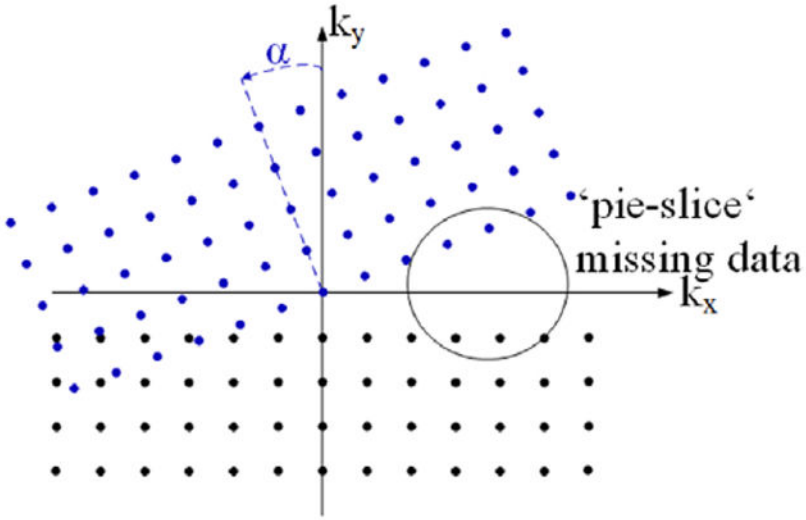

Figure 7.
Effect of rotation around the *z*-axis in image space on a 2D Cartesian *k*-space.

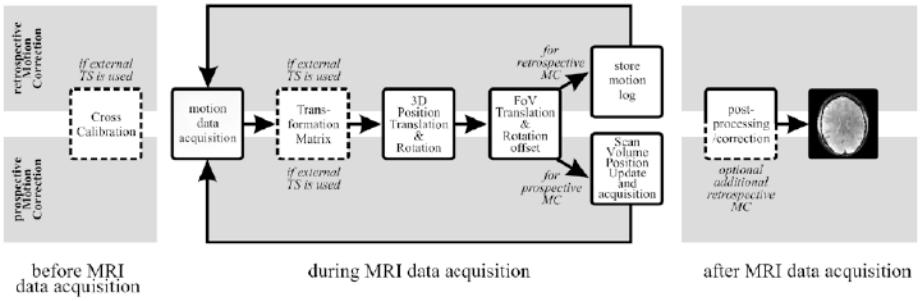

Figure 8.

Prospective motion correction pipeline: motion data has to be delivered in scanner coordinates, or at least the sequence needs the means, to convert the pose to scanner coordinates, e.g. via a transformation matrix. Therefore, cross calibration is necessary for external tracking devices. During the scan, the motion data is acquired and the latest motion pose is used to apply the required translation and rotation by adjusting the gradients and frequencies. In contrast to retrospective motion, the correction is performed during the scan which results in an instant delivery of a consistent *k*-space data and thus a corrected image with standard reconstruction. Optionally, an additional retrospective correction of residual artefacts can be performed after the scan.

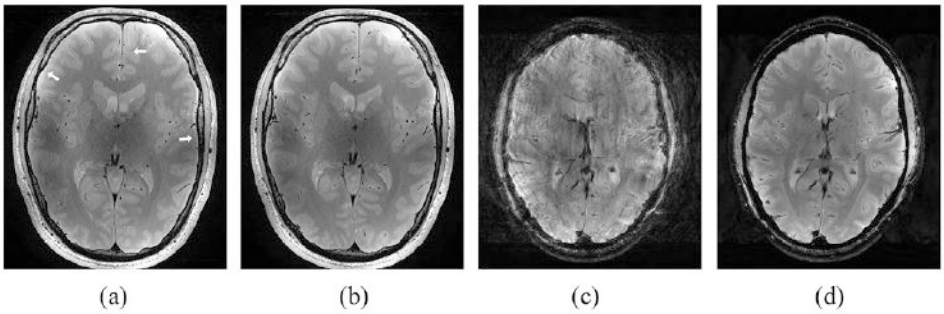

Figure 9.

Motion-corrupted and motion-corrected brain images. In high resolution images even small motion (a) can cause blurring and introduce artificial edges (see arrows) that are removed in the corrected image (b). With stronger motion (c) the image becomes largely 'non-diagnostic' with unrecognizable details that are also recovered in the corrected image (d). The images have a resolution of 0.25 mm × 0.25 mm × 2.00 mm (a), (b) and 0.28 mm × 0.28 mm × 1.00 mm (c), (d) with very similar motion within each pair.

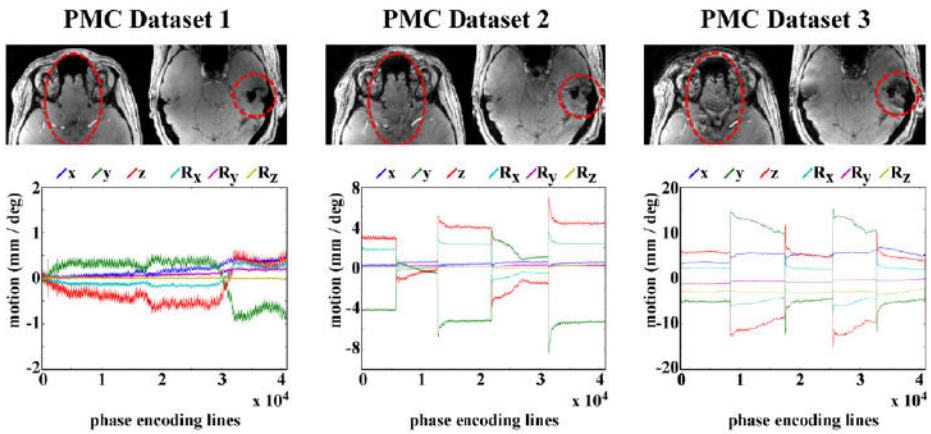

Figure 10.

The 3D SPGR images from 7T MRI show the residual artefacts after applying prospective Mo–Co under three different types of motion. The artefacts in the frontal lobes (red ovals) and temporal lobes (red circles) appear more visible with increasing motion amplitudes. Below the images are their corresponding motion patterns including 3 parameters of translation (x, y, z) and 3 parameters of rotation (R_x, R_y, R_z).